International Journal of analytical and Numerical Methods in Mechanical Design
Vol 3., Issue 1 Winter & Spring, 2024, 1-14

Free tangential vibration of cracked nanotubes incorporating scale effects using doublet mechanics

A. Fatahi-Vajari [a, *], Z. Azimzadeh [b]

[a] Department of Mechanical Engineering, Shahriar Branch, Islamic Azad University, Shahriar, Iran

[b] Department of Mathematics, Yadegar-e-Imam Khomeini (RAH) Shahre Rey Branch, Islamic Azad University, Tehran, Iran

Received 10 January 2024, Accepted 15 March 2024

Abstract

This paper investigates the free tangential vibration of cracked nanotubes with considering scale parameter under various boundary conditions. The cracked nanotube is modeled by dividing it into two segments connected by a linear spring. The stiffness of the spring is dependent to the crack severity and obtained using fracture mechanics principles. Governing equations and corresponding boundary conditions are derived with the aid of doublet mechanics (DM). The natural frequencies are obtained analytically with solving characteristics equation and the influence of the crack severity, boundary conditions, tube chirality, and the dimensions of nanotube on the free tangential vibration of cracked nanotubes is studied in detail. It was shown that the frequency decreases with increase of the crack severity and scale parameter. This reduction is more apparent when the boundaries of the beam are changed from free end to clamped one. In addition, when the crack location is near the support, a larger decrease in the frequency can be observed. To validate accuracy and efficiency of the present method, the results obtained herein are compared with the available results in the literatures and good agreement is observed.

Keywords: Tangential vibration, Cracked nanotube, Doublet mechanics, Natural frequency, Crack severity.

1. Introduction

The importance of the beam and its engineering applications is obvious, and it undergoes different kinds of loading. It is well known that presence of crack in a beam creates discontinuities varies its dynamic behavior and may cause the failure [1]. Cracks are classified base on the geometry and its orientation, cracks parallel to beam axis are known as longitudinal cracks, cracks that close and open when subjected to alternative stresses are known as breathing crack, crack which are perpendicular to the axis of shaft are known as transverse crack, the cracks on surface which is not visible known as sub-surface crack on the surface are known as surface crack. Cracked structures are susceptible to failure depending on the vibration mode. Failure is due to the resonance formed by the superposition of frequency of periodic force acting on structure and the natural frequency of the structure. Crack severity is defined by division of crack length to crack depth [2]. Natural frequency is the frequency at which a system or structure vibrates when subjected to an initial excitation in the absence of any driving or damping force [3]. Then, to determine natural frequency, free undamped vibration must be considered. For any cracked structure, the study of resonance is more important because it affects the structure in different ways [4]. When the frequency of applied load becomes equal to associated natural frequency, the structure vibrates theoretically at infinite amplitude leading to failure [5]. To avoid structural failure due to periodic load, it is important to determine resonant frequency. As material failure could lead to disastrous results, structures have regular costly and time consuming inspections. During the last decades, damage detection methods using vibration analysis have attracted growing interest because of their simplicity for implementation [6]. It is known that presence of the crack reduces its natural frequency and deviates its mode shape. It should be pointed out that the frequency reduction in cracked beam is not due to removal of mass rather the reduction of mass would increase natural frequency [7]. Indeed, a crack in a structure leads to a reduction in the stiffness and an increase in the damping of the structure. As frequencies are measured more easily than mode shapes, and on the other hand, mode shapes also affected by experimental errors, the investigation of the natural frequency is more significant. Therefore, it is possible to predict the crack depth and crack location by measuring changes in the vibration parameters.

In recent years, the study of the beamlike vibration in nanoscale devices has been of significant interest to researchers due to their use in NEMS [8]. Nowadays, it is still a challenge to study the mechanics of nanomaterials by means of experimental tests due to the difficulties exists in the nanoscale [9]. Furthermore, structures at the nanoscale are known to exhibit a size-dependent behavior. Therefore, the theoretical methods such as atomistic simulations and classical continuum mechanics (CCM) theories are often used to analyze the dynamic responses of cracked nanostructures [10- 12]. It is known that atomistic simulation methods are extremely costly and

time-consuming task [13]. On the other hand, CCM theories are assumed to be scale independence ignoring the scale effect [14]. To improve this condition, the DM elasticity theory has been also used in the linear and nonlinear vibration analysis of carbon nanotubes [15, 16]. Due to different causes, cracks are often found in the nanostructures. For example, thermally-induced crack in the fabrication process of nanomaterials such as ZnO nanorods and nanowires may be created during heating [17]. The presence of the cracks in the nanodevices affects the safety and reliability in applications. However, few published papers investigated the aspect of mechanical analysis of cracked nanostructures [18]. Another field that recently attracted growing interest for the researchers is considering the scale effects on vibration of cracked nanobeams. Recently, nonlocal beam model has been adopted for the flexural [19, 20] and torsional [21, 22] vibration analysis of cracked nanostructures. Buckling behavior of imperfect axially compressed cylinder with an axial crack studied by many researcher [23, 24]. However, fewer researches have been so far conducted on the vibration behavior of cracked CNTs using DM theory. Although, there are several studies focusing on the axial responses of these kinds of nanostructures, none of them has incorporated the scale effect, explicitly. Gheshlaghi and Hasheminejad studied the axial vibration of CNTs using a modified couple stress theory [25]. Using a nonlocal elasticity model, the effects of crack on free axial vibration of nanorods and the effects of elastic medium on axial statics and dynamics of nanotubes were investigated. Zhang et al reported an order-of-magnitude reduction in the fatigue crack propagation rate for an epoxy system with the addition of five percent of carbon nanotube additives using fractography analysis and fracture mechanics modeling [26]. Rane et al. developed a method based on measurement of natural frequencies for detection of the location and size of a crack in a cantilever beam [27]. Hsu et al. studied the longitudinal frequency of a cracked nanobeam. They obtained the frequency equation of the nanobeam with different boundary conditions based on the nonlocal elasticity theory [28]. Singh introduced transcendental eigenvalue problems in axially vibrating rods to estimate the damage parameters in the continuous structure from natural frequencies [29]. Yali and Cercevik studied the axial vibration of cracked carbon nanotubes with arbitrary boundary conditions using the nonlocal elasticity theory. The crack severity and the supports were modeled by an axial spring representing the discontinuity in the axial displacement [30]. Loghmani and Hairi Yazdi studied free vibration of Euler-Bernoulli nanobeam with multiple cracks using Eringen's nonlocal elasticity theory based on wave approach [31]. Ebrahimi and Mahmudi proposed a finite element (FE) model to study the thermal transverse vibrations of cracked nanobeams resting on a double-parameter nonlocal elastic foundation using Hamilton's principal [32]. Dilena and Morassi studied the identification of a single open crack in a vibrating beam, either under axial or bending vibration, based on measurements of damage-induced shifts in natural frequencies and antiresonant frequencies [33].

As far as known, however, there has been few investigation on the tangential vibration of a nanostructure with cracks explicitly incorporates scale effect in details. The lack prompted the authors to model the free tangential vibration of cracked nanotubes based on DM theory and to investigate the scale effects on tangential frequencies. In this paper, the tangential vibration of a cracked nanobeam with different boundary conditions is studied using DM theory. The effects of the crack parameter, crack location, and scale parameter on the vibration frequency of the cracked nanotube are studied. The main purpose of the present work is to propose a comprehensive analytical model to study the free tangential vibration of cracked CNTs. To this end, the governing equations of cracked nanotubes incorporating scale effects are derived using DM principle.

2. Free tangential vibration equation of motion for SWCNT using DM

Originally developed by Granik (1978), DM is a micromechanical theory wherein solids are represented as arrays of points or nodes at finite distances. A pair of such nodes is referred to as a doublet and the nodal spacing distances introduce length scales into the microstructural theory. Each node in the array is allowed to have translation and rotation where small translational and rotational displacements are expanded in a convergent Taylor series about the nodal point. The order at which the series is truncated defines the degree of approximation employed. The lowest order case using only a single term in the series does not contain any length scales, while the terms beyond the first produce a multi-scale theory. In this way, kinematical microstrains of elongation, shear and torsion (about the doublet axis) are developed. Through appropriate constitutive assumptions, such microstrains can be related to the corresponding elongational, shear and torsional microstresses.

A doublet being a basic constitutive unit in DM is shown in Fig. 1. Corresponding to the doublet (A,B), there exists a doublet or branch vector $\boldsymbol{\zeta}_a$ connecting the adjacent particle centers and defining the doublet axis. The magnitude of this vector $\eta_a = |\boldsymbol{\zeta}_a|$ called length scales simply the particle diameter for particles in contact. However, in general, the particles need not be in contact, and for this case the length scale η_a could be used to represent a more general microstructural feature.

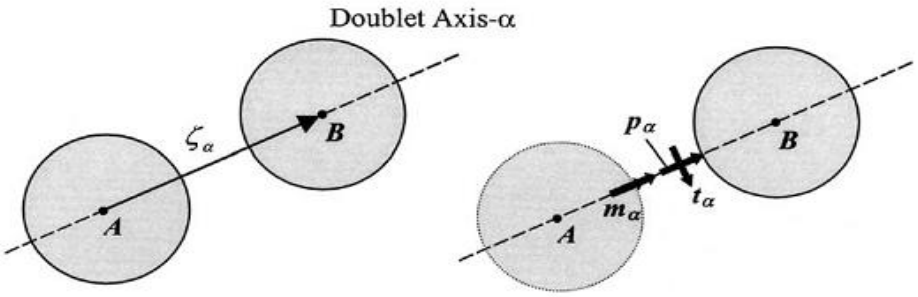

Fig 1. Doublet.

As mentioned above, the kinematics allow relative elongational, shearing and torsional motions between the particles, and this is used to develop an elongational microstress p_a, shear microstresst_a, and torsional microstressm_a as shown in Fig. 1. It should be pointed out that these microstresses are not second order tensors in the usual continuum mechanics sense. Rather, they are vector quantities that represent the elastic microforces and microcouples of interaction between doublet particles, examples of which include the interatomic forces between carbon molecules of a nanotube. The directions of microstresses depend on the doublet axes which are determined by the material microstructure. The microstresses are not continuously distributed but rather exist only at particular points in the medium being modeled by DM.

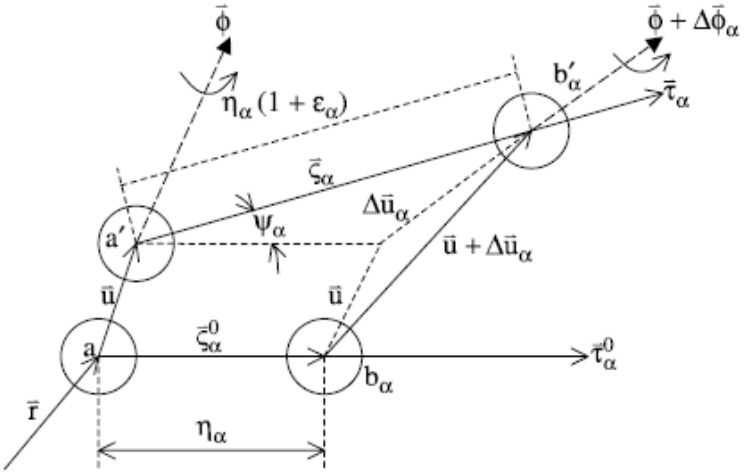

Fig 2. Translations of the doublet nodes a and b_a .

In Fig. 2, doublet (a, b_α) is shown to transform to doublet (a', b_α) as a result of kinematic translation. The superscript *0* for vectors indicates the initial configuration.

If $\boldsymbol{u}(\boldsymbol{x},t)$ is the displacement field representing the translation of node a, the incremental displacement may be written as:

$$\Delta\boldsymbol{u}_\alpha = \boldsymbol{u}\left(\boldsymbol{x}+\boldsymbol{\zeta}^0_\alpha, t\right) - \boldsymbol{u}\left(\boldsymbol{x},t\right) \tag{1}$$

where $\boldsymbol{x}$ is the position vector of the particle.

Here, $\alpha = 1,...,n$ while *n* is referred to the numbers of doublets. For the problem under study, it is assumed that the shear and torsional microdeformations and microstresses are negligible therefore only extensional microstrains and microstresses are assumed to exist.

It is further assumed that the relative displacement $\Delta\boldsymbol{u}_\alpha$ is small compared to the doublet separation distance η_α ($|\Delta\boldsymbol{u}_\alpha| \ll \eta_\alpha$) whereby it may be concluded that the unit vector $\boldsymbol{\tau}_\alpha = \boldsymbol{\tau}^0_\alpha$ [16].

The extensional microstrain scalar measure ε_α, representing the tangential deformation of the doublet vector, is defined as [15]:

$$\varepsilon_\alpha = \frac{\boldsymbol{\tau}_\alpha . \Delta\boldsymbol{u}_\alpha}{\eta_\alpha} \tag{2}$$

The incremental function in Eq. (2) is assumed to have a convergent Taylor series expansion written as [3]:

$$\varepsilon_\alpha = \sum_{\chi=1}^{M} \frac{(\eta_\alpha)^{\chi-1}}{\chi!} \boldsymbol{\tau}^0_\alpha . \left(\boldsymbol{\tau}^0_\alpha . \nabla\right)^\chi \boldsymbol{u} \tag{3}$$

where ∇ is the gradient operator and η_α are the internal characteristic length scales. As mentioned above, the number of terms used in the series expansion of the local deformation field determines the order of the approximation in DM.

In DM, the relation between microstrain and microstress, neglecting torsional and shearing microstrain and temperature effects, is written as [15]:

$$p_\alpha = \sum_{\beta=1}^{n} A_{\alpha\beta} \varepsilon_\beta \tag{4}$$

where p_α is the tangential microstress along the doublet axes. An example of the tangential microstress is the interatomic force between atoms or molecules located at the nodes of a general array such as a crystalline lattice. Eq. (4) can be interpreted as the constitutive equation in the linear theory of DM and $A_{\alpha\beta}$ is the matrix of the micromoduli of the doublet. The material is homogeneous if the matrix $A_{\alpha\beta}$ is constant throughout the body.

The unit vector $\boldsymbol{\tau}_{\alpha_0}^0$, known as the director vector, may be written as $\boldsymbol{\tau}_\alpha^0 = \tau_{\alpha j}^0 \boldsymbol{e}_j, j = 1,2,3$ where $\tau_{\alpha j}^0, j = 1,2,3$ are the cosines of the angles between the direction of the microstress vector and the coordinates and $\boldsymbol{e}_i, i = 1,2,3$ are the unit vectors of the coordinate system.

In an isotropic medium capable of undergoing only local interactions, Eq. (4) is simplified as [8]:

$$p_\alpha = A_0 \varepsilon_\alpha \tag{5}$$

The relation between macrostresses and microstresses is written as [15]:

$$\sigma_{ij}^{(M)} = \sum_{\alpha=1}^{n} \tau_{\alpha i}^0 \tau_{\alpha j}^0 \sum_{\chi=1}^{M} \frac{(-\eta_\alpha)^{\chi-1}}{\chi!} \left(\boldsymbol{\tau}_\alpha^0 . \nabla\right)^{\chi-1} p_\alpha \tag{6}$$

The superscript (*M*) in Eq. (6) refers to the generalized macrostresses which incorporate scale effects.

This macrostress in Eq. (6) is the same as stresses in virial theorem with this difference that in virial stresses, there is no gradient of microstresses and it doesn't explicitly contain scale parameter. It should be added that if the scale parameter in Eqs. (3) and (6) is set to zero, the CCM theory is obtained, as we expected.

The three-dimensional equations of motion in DM in the Cartesian coordinate system are given by [8]

$$\frac{\partial \sigma_{ij}^{(M)}}{\partial x_i} + f_i^* = \rho^* \frac{\partial^2 u_j}{\partial t^2} \tag{7}$$

where $x_i, i = 1,2,3$ are the spatial Cartesian coordinates, $u_j, j = 1,2,3$ are the displacement components, *t* is the time, and ρ^* and f^* are the three dimensional body force and mass density, respectively.

Now, the form of matrix $[\boldsymbol{A}]$ in Eq. (4) containing elastic macroconstants for a two-dimensional plane problem is obtained. For this purpose, Fig. 3 is considered wherein the $x_1 - x_2$ plane, three doublets are shown with equal angles between them.

The solution for the scale-less approximation in DM can be calculated directly from the associated continuum mechanical problem for an isotropic material.

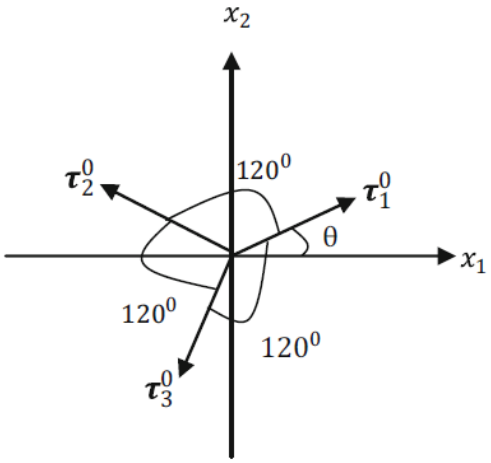

Fig 3. Three doublets with equal angle 120^0 between them.

For a two-dimensional problem in DM, the matrix $[\boldsymbol{A}]$ is a symmetric matrix of order three with the most general form [16]

$$[\boldsymbol{A}] = \begin{bmatrix} a & b & b \\ b & a & b \\ b & b & a \end{bmatrix} \tag{8}$$

It can be shown in [28] that the coefficients of tensor $[\boldsymbol{A}]$ are independent of direction thereby rendering the material isotropic. Furthermore, the coefficients a and b in matrix $[\boldsymbol{A}]$ under plane stress conditions are determined to be [8]

$$a = \frac{4}{9}\mu \frac{7\lambda + 10\mu}{\lambda + 2\mu}, b = \frac{4}{9}\mu \frac{\lambda - 2\mu}{\lambda + 2\mu} \tag{9}$$

One could use $b = 0$ as a quantitative guide to the applicability of a simpler constitutive relations such as Eq. (5). If $\lambda = 2\mu$ (or $\nu = \frac{1}{3}$) under plane stress conditions, from Eq. (9), it is concluded that $b = 0$ and

$$a = A_0 = \frac{8\mu}{3} = \frac{8G}{3} = E \tag{10}$$

Specific applications of DM have been developed for two-dimensional problems with regular particle packing microstructures. In particular, the two-dimensional hexagonal packing microstructure without internal atoms establishes three doublet axes at 120^0 angles as shown in Fig. 3.

In the remainder of this section, the governing equations for tangential vibration of SWCNTs are derived. Now, consider a SWCNT of length *L*, mean radius *R*, Young's modulus *E*, Poisson's ratio ν and mass density ρas shown in Fig. 4.

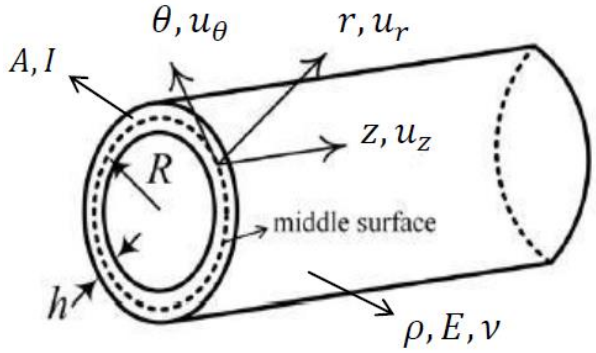

Fig 4. A nanotube in cylindrical coordinate.

In the cylindrical coordinates, the equations of motion are given by the following equations [16]

$$\frac{\partial N_{zz}}{\partial z}+\frac{1}{r}\frac{\partial N_{\theta z}}{\partial \theta}+\rho f_z=\rho\frac{\partial^2 u_z}{\partial t^2} \tag{11}$$

$$\frac{\partial N_{z\theta}}{\partial z}+\frac{1}{r}\frac{\partial N_{\theta\theta}}{\partial \theta}+\frac{N_{\theta r}}{r}+\rho f_\theta=\rho\frac{\partial^2 u_\theta}{\partial t^2} \tag{12}$$

$$\frac{\partial N_{zr}}{\partial z}+\frac{1}{r}\frac{\partial N_{\theta r}}{\partial \theta}-\frac{N_{\theta\theta}}{r}+\rho f_r=\rho\frac{\partial^2 u_r}{\partial t^2} \tag{13}$$

$$\frac{\partial M_{zz}}{\partial z}+\frac{1}{r}\frac{\partial M_{\theta z}}{\partial \theta}+\rho\bar{l}_z=N_{zr} \tag{14}$$

$$\frac{\partial M_{z\theta}}{\partial z}+\frac{1}{r}\frac{\partial M_{\theta\theta}}{\partial \theta}+\frac{1}{r}M_{\theta r}+\rho\bar{l}_\theta=N_{\theta r} \tag{15}$$

$$\frac{M_{zr}}{\partial z}+\frac{1}{r}\frac{M_{\theta r}}{\partial \theta}-\frac{M_{\theta\theta}}{r}+\rho\bar{l}_r=N_{rr} \tag{16}$$

which are the equations of motion of a thin shell in the cylindrical coordinates.

Also, assuming that the shell-like body is thin, Eqs. (17) and (18) may be used to write the physical components N_{ij} and M_{ij} as:

$$N_{ij}=\int_{-\frac{h}{2}}^{\frac{h}{2}}\sigma_{ij}^{(M)}dz\ ,i,j=1,2,3 \tag{17}$$

$$M_{ij}=\int_{-\frac{h}{2}}^{\frac{h}{2}}z\sigma_{ij}^{(M)}dz\ ,i,j=1,2,3 \tag{18}$$

From Eq. (3), the microstrains with only three terms in the expansion can be written in cylindrical coordinates as:

$$\varepsilon_\alpha=\boldsymbol{\tau}_\alpha^0.\left(\boldsymbol{\tau}_\alpha^0.\nabla\boldsymbol{u}\right)+\frac{1}{2}\eta_\alpha\left[\boldsymbol{\tau}_\alpha^0.\left(\boldsymbol{\tau}_\alpha^0.\nabla\right)\left(\boldsymbol{\tau}_\alpha^0.\nabla\boldsymbol{u}\right)\right]+\frac{1}{6}\eta_\alpha^2\left[\boldsymbol{\tau}_\alpha^0.\left(\boldsymbol{\tau}_\alpha^0.\nabla\right)\left(\boldsymbol{\tau}_\alpha^0.\nabla\right)\left(\boldsymbol{\tau}_\alpha^0.\nabla\boldsymbol{u}\right)\right] \tag{19}$$

where the gradient operator ∇ in cylindrical coordinates is given by

$$\nabla=\frac{\partial}{\partial r}\boldsymbol{e}_r+\frac{1}{r}\frac{\partial}{\partial\theta}\boldsymbol{e}_\theta+\frac{\partial}{\partial z}\boldsymbol{e}_z \tag{20}$$

Similarly, from Eq. (6), the macro- to microstress relations, to within three terms in the expansion, in the cylindrical coordinates may be written as:

$$\boldsymbol{\sigma}^{(M)}=\sum_{\alpha=1}^{n}\boldsymbol{\tau}_\alpha^0\boldsymbol{\tau}_\alpha^0\left\{\left(p_\alpha-\frac{1}{2}\eta_\alpha\boldsymbol{\tau}_\alpha^0.\left(\nabla p_\alpha\right)+\frac{1}{6}\eta_\alpha^2\left[\left(\boldsymbol{\tau}_\alpha^0.\nabla\right)\left(\boldsymbol{\tau}_\alpha^0.\nabla p_\alpha\right)\right]\right)\right\} \tag{21}$$

In this study, the following assumptions, known as Love's first approximation, for cylindrical shells are made:

1. All points that lie on a normal to the middle surface before deformation do the same after the deformation. Then the transverse shear stresses $\sigma_{rz}^{(M)}$ and $\sigma_{\theta z}^{(M)}$ are assumed to be negligible.
2. Displacements are small compared to the shell thickness.
3. The normal stresses in the thickness direction ($\sigma_{rr}^{(M)}$) are negligible (planar state of stress).

It should be mentioned that in the tangential vibration, the nanotube vibrates in the tangential direction. Let the nanotube is approximated by a homogeneous cylinder. Thus, with assumptions of homogeneity for the entire tube in the tangential vibration, this implies that $\frac{\partial}{\partial z}=0,\frac{\partial}{\partial r}=0$ and $u_r=0,u_z=0$. Considering such

assumptions and neglecting body forces, Eqs. (32)- (37) reduce to

$$\frac{\partial N_{z\theta}}{\partial z}+\frac{1}{r}\frac{\partial N_{\theta\theta}}{\partial \theta}+\frac{N_{\theta r}}{r}+\rho f_{\theta}=\rho\frac{\partial^2 u_{\theta}}{\partial t^2} \qquad (22)$$

As a result of the above assumptions, the gradient operator and the displacement vector are given by:

$$\nabla=\frac{1}{r}\frac{\partial}{\partial\theta}\boldsymbol{e}_{\theta},\boldsymbol{u}=u_{\theta}(\theta)\boldsymbol{e}_{\theta} \qquad (24)$$

It is further assumed that all doublets originating from a common node have the same magnitudes, i.e., $\eta_a=\eta, a=1,2,3.$

As mentioned above, a SWCNT is constructed from three doublets having equal lengths and angles between them, an example of which is a Zigzag SWCNT ($\theta=0$ in Fig. 3) shown in Fig. 5.

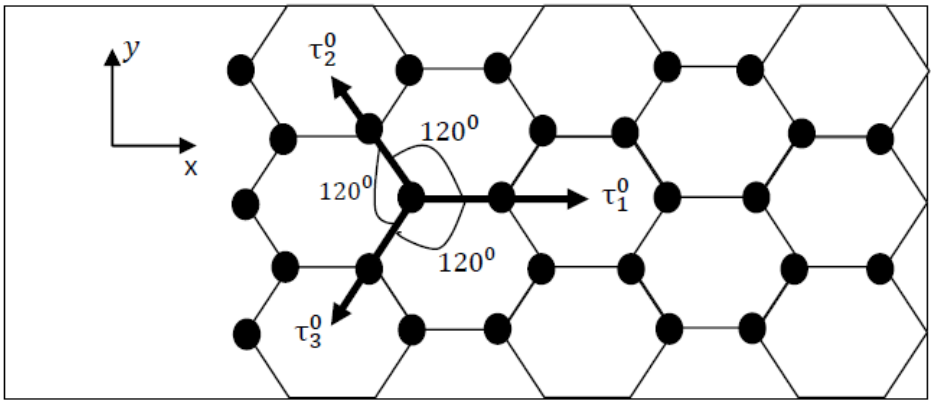

Fig 5. A Zigzag nanotube.

Considering Fig. 5, the director vectors in cylindrical coordinates can be expressed as:

$$\tau_{1r}^0=0,\tau_{2r}^0=0,\tau_{3r}^0=0 \qquad (25)$$

$$\tau_{1\theta}^0=0,\tau_{2\theta}^0=cos30,\tau_{3\theta}^0=-cos30 \qquad (26)$$

$$\tau_{1z}^0=-1,\tau_{2z}^0=-cos60,\tau_{3z}^0=-cos60 \qquad (27)$$

where z is in the tangential direction and r and θ are in the radial and circumferential directions of the nanotube, respectively.

For Armchair one, the director vectors in cylindrical coordinates reduced to

$$\tau_{1r}=0,\tau_{2r}=0,\tau_{3r}=0 \qquad (28)$$

$$\tau_{1\theta}=1,\tau_{2\theta}=-cos60,\tau_{3\theta}=-cos60 \qquad (29)$$

$$\tau_{1z}=0,\tau_{2z}=cos30,\tau_{3z}=-cos30 \qquad (30)$$

Substituting Eq. (24) into Eq. (19) and performing some algebraic manipulations detailed in Appendix A, it is found that

$$\epsilon_{\alpha}=\frac{1}{r}(\tau_{\alpha\theta}^0)^2\frac{\partial u_{\theta}}{\partial\theta}+\frac{1}{2}\eta_{\alpha}\left[\frac{1}{r^2}(\tau_{\alpha\theta}^0)^3\left(\frac{\partial^2 u_{\theta}}{\partial\theta^2}-u_{\theta}\right)\right]+\frac{1}{6}\eta_{\alpha}^2\left[\frac{1}{r^3}(\tau_{\alpha\theta}^0)^4\left(\frac{\partial^3 u_{\theta}}{\partial\theta^3}-3\frac{\partial u_{\theta}}{\partial\theta}\right)\right] \qquad (31)$$

Inserting Eq. (31) into Eq. (4), the following equation for the microstresses is obtained

$$p_{\alpha}=A_0\left\{\frac{1}{r}(\tau_{\alpha\theta}^0)^2\frac{\partial u_{\theta}}{\partial\theta}+\frac{1}{2}\eta_{\alpha}\left[\frac{1}{r^2}(\tau_{\alpha\theta}^0)^3\left(\frac{\partial^2 u_{\theta}}{\partial\theta^2}-u_{\theta}\right)\right]+\frac{1}{6}\eta_{\alpha}^2\left[\frac{1}{r^3}(\tau_{\alpha\theta}^0)^4\left(\frac{\partial^3 u_{\theta}}{\partial\theta^3}-3\frac{\partial u_{\theta}}{\partial\theta}\right)\right]\right\} \qquad (32)$$

Similarly, substituting p_{α} from Eq. (32) into Eq. (6) and taking note of Eq. (24), it is found that

$$\sigma_{ij}^{(M)}=A_0\sum_{\alpha=1}^{3}\tau_{\alpha i}^0\tau_{\alpha j}^0\left\{\frac{1}{r}(\tau_{\alpha\theta}^0)^2\frac{\partial u_{\theta}}{\partial\theta}+\frac{1}{12}\eta_{\alpha}^2\left[\frac{1}{r^3}(\tau_{\alpha\theta}^0)^4\left(\frac{\partial^3 u_{\theta}}{\partial\theta^3}-3\frac{\partial u_{\theta}}{\partial\theta}\right)\right]\right\} \qquad (33)$$

This equation is the relation between the macrostresses and the displacements. Setting i and j equal to θ in Eq. (33), the following equation for the normal stress $\sigma_{\theta\theta}^{(M)}$ is found to be

$$\sigma_{\theta\theta}^{(M)}=A_0\sum_{\alpha=1}^{3}\left\{\frac{1}{r}(\tau_{\alpha\theta}^0)^4\frac{\partial u_{\theta}}{\partial\theta}+\frac{1}{12}\eta_{\alpha}^2\left[\frac{1}{r^3}(\tau_{\alpha\theta}^0)^6\left(\frac{\partial^3 u_{\theta}}{\partial\theta^3}-3\frac{\partial u_{\theta}}{\partial\theta}\right)\right]\right\} \qquad (34)$$

If Eq. (34) are substituted into Eq. (22) and then integrated along the tube thickness, the following equation is obtained

$$\frac{\partial N_{\theta\theta}^{(M)}}{\partial\theta}=\frac{1}{r}\frac{\partial^2 u_{\theta}}{\partial\theta^2}+\frac{1}{12}\eta^2\left[\frac{1}{r^3}k\left(\frac{\partial^4 u_{\theta}}{\partial\theta^4}-3\frac{\partial^2 u_{\theta}}{\partial\theta^2}\right)\right] \qquad (35)$$

Inserting Eq. (34) into Eq. (35), the following equation is obtained

$$\frac{E}{r^2(1-\nu^2)}\left\{\frac{\partial^2 u_{\theta}}{\partial\theta^2}+\frac{1}{12}\left(\frac{\eta}{r}\right)^2\left[k\left(\frac{\partial^4 u_{\theta}}{\partial\theta^4}-3\frac{\partial^2 u_{\theta}}{\partial\theta^2}\right)\right]\right\}=\rho\frac{\partial^2 u_{\theta}}{\partial t^2} \qquad (36)$$

In DM, basic equations of scaling microdynamics for local interactions with homogeneous medium can be written as follow [15]

$$\rho\ddot{u}_i = \sum_{\kappa=2,4,\dots}^{R=2M} C_{ijk_1k_2\dots k_\kappa} \frac{\partial^\kappa u_i}{\partial x_{k_1}\partial x_{k_2}\dots\partial x_{k_\kappa}} = C_{ijkl}u_{j,kl} + C_{ijklrs}u_{j,klrs} + C_{ijklrspq}u_{j,klrspq} + \cdots \quad (37)$$

where

$$C_{ijk_1k_2\dots k_\kappa} = 2A_0 \sum_{\alpha=1}^{n} \tau_{\alpha i}^{0}\tau_{\alpha j}^{0}\tau_{\alpha k_1}^{0}\tau_{\alpha k_2}^{0}\dots\tau_{\alpha k_\kappa}^{0}\frac{\eta_\alpha^{\kappa-2}}{\kappa!} \quad (38)$$

For tangential vibration mode of SWCNTs studied in this paper, Eq. (37) is reduced to Eqs. (36). It is noted that the nonscale macromodulus C_{ijkl}, corresponding to $\kappa = 2$, is indeed independent of θ, i.e., isotropic in the plane. On the contrary, the macromoduli $C_{ijk_1k_2\dots k_\kappa}$ for $\kappa = 4,6,\dots$ are anisotropic. Then, it may be concluded that in the first approximation, $\kappa = 2$, Eq. (37) model the continuum-like behavior of solids, whereas in the other approximations, $\kappa = 4,6,\dots$ Eq. (37) also reflect discrete-like features of the solid, in a manner that increases with κ [16]. Therefore, it can be concluded that DM is capable of modeling solids in view of their dual and to some extent contradictory discrete continuous nature. The power of such dual-representation capability is evident in the discussion of isotropy. The basal plane of the doublets arrangement (Fig. 3) is isotropic only in the continuum (nonscale) approximation. Thus, isotropy is a scale-related notion. In fact, no material may be argued to be isotropic at all dimensional scales, down to its most elementary component level [15].

3. Crack modeling

A schematic diagram of a cracked nanobeam is depicted in Fig 6. The nanobeam with previous specifications has a crack at location C located at a distance L_C from the left end. The crack is modeled by a linear elastic spring representing the discontinuity in the tangential displacement. Crack severity or crack parameter shown with K defined by $K = \frac{EA}{kL}$. In the present model, the effect of the crack is taken into account following the methodology proposed in [28]. To this end, the CNT is divided into two intact nanobeam pieces which are connected by an spring located at the cracked section to consider the additional strain energy due to the presence of the crack. It is obvious that in the crack location, the tangential displacement has discontinuity. However the tangential force is presumed to be continuous. Natural frequencies for cracked nanobeams for different crack positions, crack severities, mode numbers, and dimensions of nanobeam on the free tangential vibration of nanotubes are studied. In this work, the nanobeam with a single and double edge crack for a tangential vibration is explored based on the DM theory.

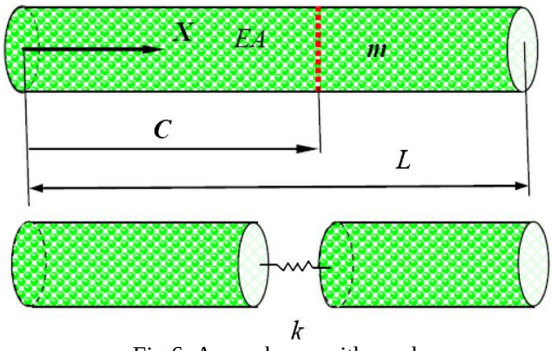

Fig 6. A nanobeam with crack

It should be pointed out that presence of crack causes a complex geometrical property which is difficult to study. Analyzing the results in the presence of the crack, the equation of motion for two intact nanobeams given with Eq. (36) can be expressed as [3]

$$\frac{E}{r^2(1-\nu^2)}\left\{\frac{\partial^2 u_{1\theta}}{\partial\theta^2} + \frac{1}{12}\left(\frac{\eta}{r}\right)^2\left[k\left(\frac{\partial^4 u_{1\theta}}{\partial\theta^4} - 3\frac{\partial^2 u_{1\theta}}{\partial\theta^2}\right)\right]\right\} = \rho\frac{\partial^2 u_{1\theta}}{\partial t^2} \quad (39)$$

$$\frac{E}{r^2(1-\nu^2)}\left\{\frac{\partial^2 u_{2\theta}}{\partial\theta^2} + \frac{1}{12}\left(\frac{\eta}{r}\right)^2\left[k\left(\frac{\partial^4 u_{2\theta}}{\partial\theta^4} - 3\frac{\partial^2 u_{2\theta}}{\partial\theta^2}\right)\right]\right\} = \rho\frac{\partial^2 u_{2\theta}}{\partial t^2} \quad (40)$$

The solution of Eqs. (39) and (40) can be expressed as

$$u_{1\theta} = A_1 sin\left(\frac{\omega_n}{\omega}\theta\right) + B_1 cos\left(\frac{\omega_n}{\omega}\theta\right) \quad (41)$$

$$u_{2\theta} = A_2 sin\left(\frac{\omega_n}{\omega}\theta\right) + B_2 cos\left(\frac{\omega_n}{\omega}\theta\right) \quad (42)$$

wherein $\omega = \frac{E}{\rho r^2(1-\nu^2)}$ indicate the natural frequency without considering crack, mode number and scale parameter. ω_n is the frequency incorporating scale effect, mode number and crack severity.

Eqs (39) and (40) are the free tangential vibration solution of the segment one and two, respectively. Eqs. (41) and (42) have four unknown coefficients must be determined. Obtaining the natural frequencies in tangential mode, two more conditions than boundary conditions are needed. The conditions are compatibility conditions at the crack section given by:

Jump in tangential deflection,

$$u_{1\theta} - u_{2\theta} = CF_{1\theta} \quad (43)$$

Continuity of the tangential force,

$$F_{1\theta} = F_{2\theta} \quad (44)$$

In Eq. (43), $C = \frac{1}{k}$ is the flexibility of the spring and obtained using fracture mechanics principles.

$$F_\theta = \frac{EA}{1-\nu^2}\left\{\frac{\partial u_\theta}{\partial\theta} + \frac{1}{12}\eta^2\left[k\frac{1}{r^3}\left(\frac{\partial^3 u_\theta}{\partial\theta^3} - 3\frac{\partial u_\theta}{\partial\theta}\right)\right]\right\} \quad (45)$$

Applying the boundary and compatibility conditions, Eqs. (43) and (44) yield a system of four homogeneous algebraic equations with A_1, B_1, A_2, and B_2 as unknowns. For two ends clamped boundary conditions, Eqs. (43) and (44) can be written in matrix form as

$$\begin{bmatrix} -Cu & 1 & 0 & -1 \\ u & 0 & u & 0 \\ \sin\left(\frac{\omega_n}{\omega}\pi\right) - Cu & \cos\left(\frac{\omega_n}{\omega}\pi\right) + Cu & -\cos\left(\frac{\omega_n}{\omega}\pi\right) & -\cos\left(\frac{\omega_n}{\omega}\pi\right) \\ u\cos\left(\frac{\omega_n}{\omega}\pi\right) & u\sin\left(\frac{\omega_n}{\omega}\pi\right) & -u\cos\left(\frac{\omega_n}{\omega}\pi\right) & -u\sin\left(\frac{\omega_n}{\omega}\pi\right) \end{bmatrix} \begin{bmatrix} A_1 \\ B_1 \\ A_2 \\ B_2 \end{bmatrix} = 0 \qquad (46)$$

wherein $u = \frac{EA}{1-\nu^2}\left\{\frac{\omega_n}{\omega} + \frac{1}{12}\eta^2 k \frac{1}{r^3}\left[\left(-\left(\frac{\omega_n}{\omega}\right)^3 - 3\frac{\omega_n}{\omega}\right)\right]\right\}$

For a nontrivial solution of A_1, B_1, A_2 and B_2, the determinant of the coefficients of the matrix must be set to zero for each boundary type. The process gives the explicit form of characteristic equation of the cracked nanobeam with fixed-fixed yields

$$D = \begin{vmatrix} -Cu & 1 & 0 & -1 \\ u & 0 & u & 0 \\ \sin\left(\frac{\omega_n}{\omega}\pi\right) - Cu & \cos\left(\frac{\omega_n}{\omega}\pi\right) + Cu & -\cos\left(\frac{\omega_n}{\omega}\pi\right) & -\cos\left(\frac{\omega_n}{\omega}\pi\right) \\ u\cos\left(\frac{\omega_n}{\omega}\pi\right) & u\sin\left(\frac{\omega_n}{\omega}\pi\right) & -u\cos\left(\frac{\omega_n}{\omega}\pi\right) & -u\sin\left(\frac{\omega_n}{\omega}\pi\right) \end{vmatrix} = 0 \qquad (47)$$

One may introduce the frequency ratio as the frequency of nanobeam without considering crack to the frequency of the cracked nanobeam to obtain dimension less frequency as

$$F.R = \frac{Natrual\ Frequency\ without\ crack}{Natrual\ Frequency\ with\ crack} \qquad (48)$$

The roots of the characteristic equation (47) are the tangential frequencies for the cracked nanobeam incorporating the scale effects, explicitly. A MATLAB program is written to solve the characteristic equations. It should be pointed out here that, by setting $C = 0$ in the above equations, it can be obtained the natural frequency, i.e. eigenvalue equations, of the corresponding uncracked nanobeams and $\eta = 0$ the corresponding scale less nanobeam. Indeed, the computation of these vibration frequencies may also be used to detect the location and severity of cracks in a nanostructure.

4. Local flexibility of cracked nanostructure

Assume that a slender prismatic nanobeam with a circular cross section, having a non-propagating single or double edge crack (SEC or DEC) (or flaw like crack) are shown in Fig. 7.

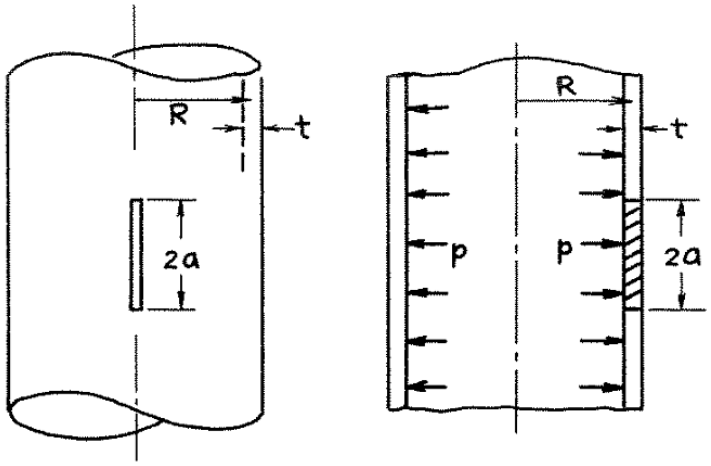

Fig 7. DEC in tangential loading of SWCNT

The cracked section is presented by a massless spring with flexibility C, where

$$F = k\Delta x \qquad (49)$$

And

$$C = \frac{1}{k} = \frac{\Delta x}{F} \qquad (50)$$

This quantity is a function of the crack severity and the stiffness (EA) of the cross section of the nanobeam, and can be written as suggested in [24] as below:

$$C = \frac{d}{EA} f(\xi) \qquad (51)$$

wherein $f(\xi)$ is calculated by the following equations

For single edge crack (SEC)

$$f(\xi) = 0.0007 + 0.3255\xi - 8.4253\xi^2 + 167.486\xi^3 - 831.418\xi^4 + 2268.89\xi^5 - 3154.06\xi^6 + 1852.87\xi^7 \qquad (52)$$

For double edge crack (DEC)

$$f(\xi) = -0.0445 + 11.77\xi - 393.721\xi^2 + 4813.5\xi^3 - 27314.8\xi^4 + 79935\xi^5 - 115803\xi^6 + 66031.8\xi^7 \qquad (53)$$

where d is the diameter of the circular cross section and $f(\xi)$ is called the local flexibility function.

In this study an attempt is also made to calculate the stress intensity factor of the nanobeam explicitly incorporate scale effect using DM and principals of fracture mechanics. The predictive equation $f(\xi)$ for slender prismatic nanobeam with a SEC and DEC is proposed as [34]

$$K_I = \sigma\sqrt{\pi a} F(\gamma), \gamma = \frac{a}{\sqrt{Rt}} \qquad (54)$$

wherein $F(\gamma)$ is a function of crack severity and crack type defined by the following equations for cracked nanobeam with circular cross section.
For single edge crack

$$F(\gamma) = \begin{cases} \sqrt{1 + 1.25\gamma^2} & 0 < \gamma \leq 1 \\ 0.6 + 0.9\gamma & 1 \leq \gamma \leq 5 \end{cases} \quad (55)$$

5. Results and discussion

In order to validate the presented method, as well as to demonstrate their implementation to dynamical analysis, a cracked nanotube with free boundary condition is considered. The crack parameter K is taken as 0.000001 for noncracked nanotube. Table 1 shows the tangential frequencies of 15 different Zigzag and Armchair SWCNTs based on the available experimental and analytical results. The first column shows the n and m chiral indices of the nanotube; the second column shows the SWCNT diameter (d, in nm) and the next three columns are the experimental, analytical and the present method results, respectively. From this Table, it can be seen that the doublet mechanical predictions of the tangential frequencies of different SWCNTs are in good agreement with the available results.

Tube (n, m)	Diameter (nm)	Experiment [25]	Shell theory [19]	DM (present work)
(6,0)	0.4698	475.7	480.9	469.8
(7,0)	0.5481	407.8	412.2	405.3
(8,0)	0.6264	356.8	360.7	356.0
(9,0)	0.7047	317.2	320.6	317.4
(10,0)	0.7830	285.4	288.6	286.2
(11,0)	0.8613	259.5	262.3	260.5
(12,0)	0.9397	237.8	240.5	239.1
(13,0)	1.0180	219.5	222.0	220.9
(14,0)	1.0963	203.9	206.1	205.2
(15,0)	1.1746	190.3	192.4	191.7
(16,0)	1.2529	178.4	180.4	179.8
(17,0)	1.3312	167.9	169.7	169.3
(18,0)	1.4095	158.6	160.3	159.9
(19,0)	1.4878	150.2	151.9	151.5
(20,0)	1.5661	142.7	144.3	144.0

Experimentally, the tangential frequency is related to ω via $f = \frac{\omega}{2\pi C}$ where, $C = 2.99 \times 10^{10} \frac{cm}{s}$ is the velocity of light in the vacuum. This relation is used in Table 1 below to report the frequencies in cm^{-1}. Throughout this paper, the material properties of SWCNT are taken to be: Young's modulus $E = 1\,TPa$, mass density $\rho = 2300\ \frac{kg}{m^3}$ and Poisson's ratio $\nu = 0.2$ [19]. In the DM model, the scale parameter used is the carbon-carbon bond length $\eta = 0.1421\,nm$ [8].
In order to investigate the effect of different parameters like crack parameter, boundary condition, crack position and scale parameter to frequency in tangential vibration of cracked SWCNTs, several graphical form are depicted in Figs. 8- 11.

Effect of Crack severity and tube chirality
Fig. 8 shows that effect of crack opening size on the frequency ratio of the cracked nanobeam for Zigzag and Armchair nanotubes. The boundary condition is fixed-free and the crack is located as $\frac{L_c}{L} = 0.5$. From this figure, it can be seen that as the crack parameter increases, the frequency decreases. Moreover, this reduction is significant as the crack severity being larger. As the crack severity is more increases, the two graphs approaches to single value. That's why the smaller crack severity is used for further modeling. It can also be concluded that in identical crack severity, the frequency of Zigzag chiral is higher than the Armchair one. This increase is more apparent in lower crack severities.

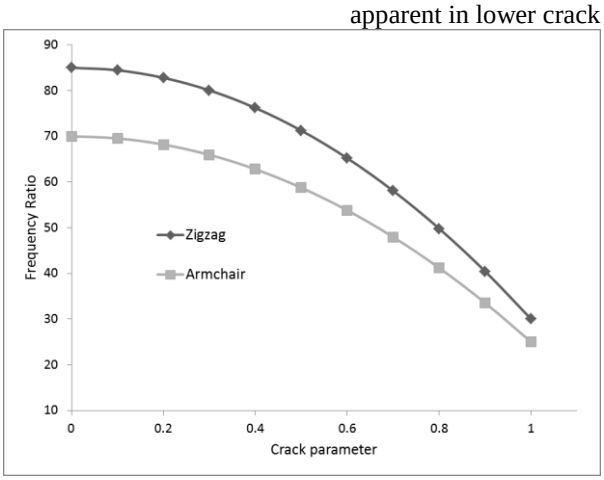

Fig 8. Natural frequency versus crack severity

Effect of boundary condition and crack location

Effect of crack location for specified scale parameter has been represented in Fig. 9 for various crack severity for fixed-free boundary condition. The crack parameter is assumed to be $K = 0.11$ and the first mode of vibration is considered. From this figure, it can be observed that frequency ratio varies for a certain crack parameter depending on the crack location. It can be seen that frequency ratio increases as the crack moves away from the fixed end. In other words, reduction in frequency is less for crack located near free end. It is also seen that as the crack severity increases, the frequency ratio decreases. This reduction is more apparent as the crack location moves to neighborhood of free end support.

This important note should be noticed carefully. As crack moves to fixed boundaries, the reduction is more apparent. To explain this effect sensibly, we can consider this example. Suppose a bar with free-free boundary conditions with a crack in the middle of the bar. As the crack moves from the middle to the end of the free boundaries, as it is expected, the effect of the crack is lessen. When crack reaches exactly to the end of the bar, it can be supposed that there is no crack in the bar. Therefore, we can conclude that as crack move to the free end boundaries, the effect of crack decreases.

Now, we can suppose a bar with fixed-fixed boundaries with a crack in the middle. In this case, as the crack moves toward the fixed end, the effect of the crack is more apparent. Especially when the crack reaches around the fixed ends of the bar, the frequency severely is affected by the crack. In this case the tube may even be separated from the support.

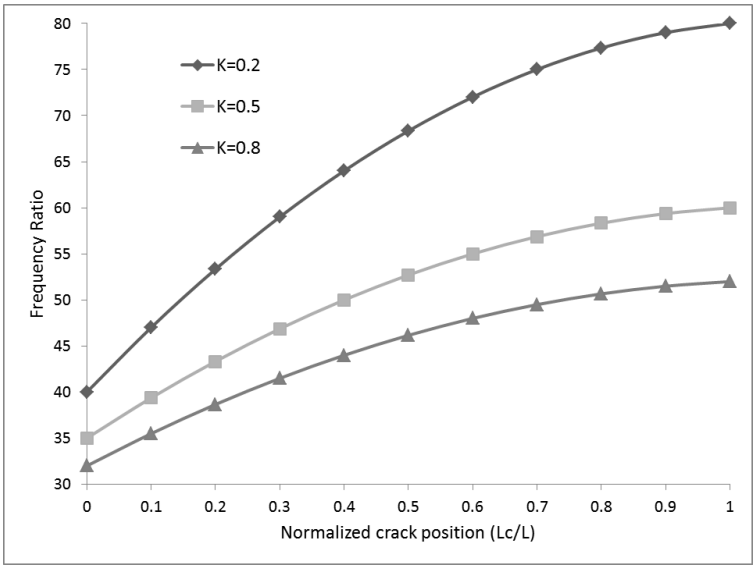

Fig 9. Frequency ratio versus normalized crack position

Effect of tube length and boundary condition

Next, the effects of the tube length on the tangential frequency are noticed. For this purpose, in Fig. 10, the frequency ratio of nanobeams with respect to tube length for different boundary condition is depicted.

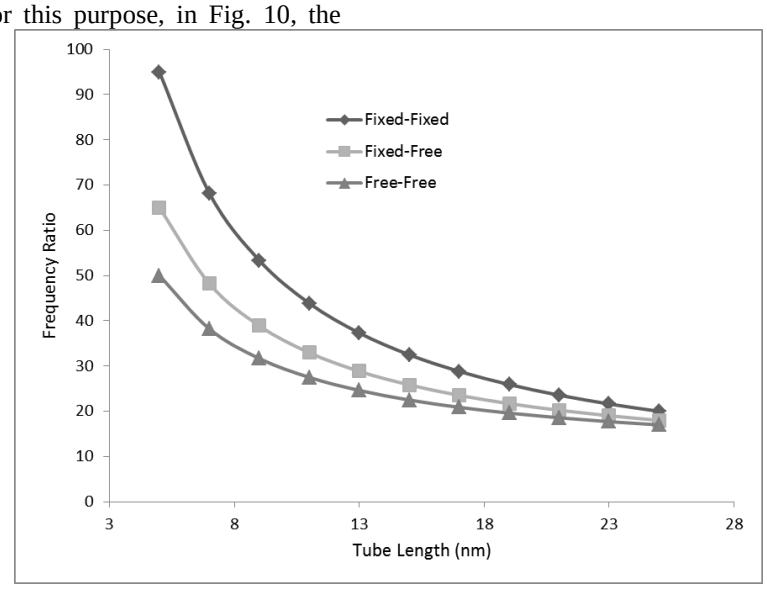

Fig 10. Frequency ratio versus tube length (A) for different mode number

From this figure, it can be concluded that fixed boundary condition is higher than free one. This difference is more apparent in lower tube length. The frequency is decreases as the tube length increases. As the tube length increases more, the difference between boundary condition decreases. In other words, for nanobeams with enough large length, the effect of the boundary condition on frequency is negligible, and only the crack can have an apparent decreasing effect on lower length.

Effect of crack type and scale parameter

To demonstrate the influence of the scale parameter on the critical stress intensity factor (also known as fracture toughness) of cracked nanobeams, variations of the Fracture toughness versus the scale parameter is plotted for different crack opening size for fixed-free boundary condition in Fig. 11. From this figure, it can be observed that fracture toughness decreases as the scale parameter increases. This reduction is more apparent in higher scale parameters. From this figure, the following important notes can be achieved. Firstly, in addition to the crack severity, the scale parameter has a decreasing effect on the tangential frequency. The decreasing effect of the crack is the result of the rigidity loss of the structure, and the more flexible the structure is, the smaller its frequency is. The decreasing effect of the scale parameter can be explained in this way that the scale has a negative modulus, and its negative amount is increased by the surface residual stress resulting in the decrease in the rigidity of nanobeam. Moreover, the scale parameter decreases the potential energy of the system, and as it is known, as the potential energy of the system decreases, its natural frequency decreases too. Then, the scale effect is taken account in the analysis that makes the nanobeam stiffer. Therefore, a larger nonlocal parameter leads to a decrease of the crack effect on the frequency.

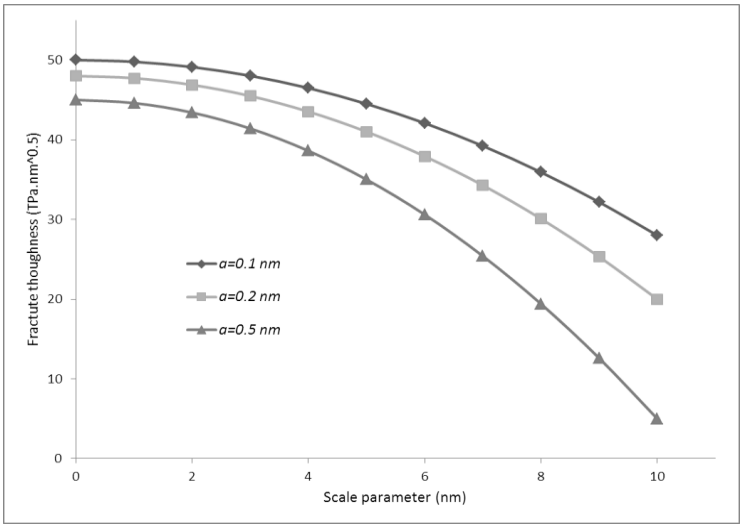

Fig 11. Fracture toughness ($TPa\sqrt{nm}$) versus scale parameter for different crack opening size

6. Conclusions

In this study, the free tangential vibration of cracked nanobeams in the presence of the scale effects is investigated using DM elasticity theory with different boundary conditions. The governing equation of motion is obtained with dividing the nanotube into two segment in crack location connected with a linear spring with flexibility determined from fracture mechanics principles. The results reveal that both the crack severity and scale parameter have a decreasing effect on the natural frequency.

From the present study, the following notes are especially obtained:

1. By using the present method, the eigenvalue equation for a cracked nanorod with any kinds of boundary conditions can be conveniently determined from a fourth order determinant.
2. The vibration frequency of nanorods is shown to be dependent on the crack severity, the end conditions and scale parameter.
3. Influence of a crack on the dynamic behavior of the nanorod is sensitive to its location and length. Natural frequency reduces due to the presence of cracks. The amount of reduction depends on location and size of cracks. As crack moves to the fixed support, more reduction in frequency is observed. On the other hands, the effect of crack is more pronounced when the cracks are near to the fixed end than at free end.
4. For a certain crack location, the natural frequencies of a cracked nanotube are inversely proportional to the crack severity. While for a certain crack severity, change in natural frequency is less as the crack position moves away from fixed end.
5. By increasing the length of the nanotube, the effect of the crack decreases. For the nanotubes with enough large length, the effect of the crack on the frequency of nanotube can be neglected.
6. In the same conditions, Armchair nanotubes has lower frequency that the Zigzag one. This

difference is more pronounced in lower cracked parameter.

7. For a certain crack parameter, change in natural frequency is less as the crack position moves away from fixed end.
8. The scale parameter has decreasing effect on fracture toughness. This reduction is more apparent in higher scale parameters.

Reference

[1] Ahmed Saimi, Ismail Bensaid and Ömer Civalek, "A study on the crack presence effect on dynamical behaviour of bi-directional compositionally imperfect material graded micro beams", Compos. Struct., Vol. 316, No. 15, pp. 1170302, (2023).

[2] K. Larkin, M. Ghommem, A. Hunter and A. Abdelkefi, "Crack severity and size dependent effects on the effectiveness and operability of micro/nanogyroscopes", Int. J. Solids Struct., Vol. 216, pp. 94-107, (2021).

[3] A. Fatahi-Vajari, A. Imam, "Axial vibration of single-walled carbon nanotubes using doublet mechanics", Indian J. Phys., Vol. 90, No. 4, pp. 447–455, (2016).

[4] Aleksandar Nikolić and Slaviša Šalinić, "Free vibration analysis of cracked beams by using rigid segment method", Appl. Math. Modell. , Vol. 84, pp. 158-172, (2020).

[5] A. Fatahi-Vajari and Z. Azimzadeh , "Analysis of nonlinear axial vibration of single-walled carbon nanotubes using Homotopy perturbation method", Indian J. Phys., November Vol. 92, No. 11, pp. 1425–1438, (2018).

[6] Seyyed Sajad Mousavi Nejad Souq, Faramarz Ashenai Ghasemi and Mir Masoud Seyyed Fakhrabadi, "A comparative study of crack detection in nanobeams using molecular dynamics, analytical and finite element methods", Journal of Computational Applied Mechanics, Vol. 52, No. 3, pp. 408-422, (2021).

[7] Siva Sankara Babu Chinka, Srinivasa Rao Putti and Bala Krishna Adavi, "Modal testing and evaluation of cracks on cantilever beam using mode shape curvatures and natural frequencies", Struct., Vol. 32, pp. 1386-1397, (2021).

[8] Alireza Fatahi-Vajari and Zahra Azimzadeh, "Axial vibration of single-walled carbon nanotubes with fractional damping using doublet mechanics", Indian J. Phys., Vol. 94, No. 7, pp. 975-986, (2019).

[9] Linda J. Johnston a, Norma Gonzalez-Rojano b, Kevin J. Wilkinson c and Baoshan Xing, "Key challenges for evaluation of the safety of engineered nanomaterials", NanoImpact, Vol. 18, pp. 100219, (2020).

[10] Md. Shumon Miaa, Md. Shahidul Islam, Udayan Ghosh, "Modal Analysis of Cracked Cantilever Beam by Finite Element Simulation", Procedia Eng., Vol. 194, pp. 509 – 516, (2017).

[11] Swapnil Dokhe and Shailesh Pimpale, "Effects of crack on modal frequency of cantilever beam", International journal of research in aeronautical and mechanical engineering, Vol.3, No. 8, pp. 24-38, (2015).

[12] P. Y. Ghodke, D. H. Tupe and G. R. Gandhe, "Modal Analysis Of Cracked Continuous Beam Using ANSYS", International Research Journal of Engineering and Technology (IRJET), Vol. 04, No. 02, pp. 86-93, (2017).

[13] Qiang Lua & Baidurya Bhattacharya, "Fracture resistance of zigzag single walled carbon nanotubes, Nanotechnology", Institute of Physics, vol. 17, pp. 1323 - 1332, (2006).

[14] Aleksandar Nikolić and Slaviša Šalinić, "Free vibration analysis of cracked beams by using rigid segment method", Appl. Math. Modell., Vol. 84, pp. 158-172, (2020).

[15] A. Fatahi-Vajari and A. Imam, "Lateral Vibrations of Single-Layered Graphene Sheets Using Doublet Mechanics", Journal of Solid Mechanics, Vol. 8, No. 4, pp. 875-894, (2016).

[16] A Fatahi-Vajari and A Imam, "Analysis of radial breathing mode of vibration of single-walled carbon nanotubes via doublet mechanics", ZAMM. Vol. 96, No. 9, pp. 1020-1032, (2016).

[17] Sri Aurobindo Panda, Sumita Choudhary, Sushil Barala, Arnab Hazra, Suchit Kumar Jena and Subhashis Gangopadhyay, "Surface energy and stress driven growth of extremely long and high-density ZnO nanowires using a thermal step-oxidation process", RSC Adv., Vol. 14, pp. 28086–28097, (2024).

[18] Bingsen Fan, Xiaolong Li, Shengjie Xu, Yanhui Zhong, Bei Zhang and Xiaofeng Liu, "Experimental Study on the Mechanical Properties of NanoSilicon Modified Polyurethane Crack Repair Materials", Processes, Vol. 12, No. 8, pp. 1735.1-1735.17, (2024).

[19] Abbas Rahi and Hamed Petoft, "Free vibration analysis of multi-cracked micro beams based on Modified Couple Stress Theory", Journal of Theoretical and Applied Vibration and Acoustics, Vol. 4, No. 2, pp. 205-222, (2018).

[20] L. Anitha and J. Sudha, "Size-dependent vibration analysis of cracked micro beams reinforced with functionally graded boron nitride nanotubes in composite structures", journal of mechanics of continua and mathematical sciences, Vol. 19, No. 3, pp. 22-39, (2024).

[21] R. Nazemnezhad and P. Fahimi, "Free torsional vibration of cracked nanobeams incorporating surface energy effects", Appl. Math. Mech. -Engl. Ed., Vol. 38, No. 2, pp. 217–230, (2017).

[22] Mustafa Ö Yayli, Suheyla Y Kandemir, and Ali E Çerçevik, "Torsional vibration of cracked carbon nanotubes with torsional restraints using Eringen's nonlocal differential model", J. Low Freq. Noise Vibr. Act. Control., Vol. 38, No. 1, pp. 70-87, (2019).

[23] O. Ifayefunmi and S.H. Sheikh Md Fadzullah, "Buckling behaviour of imperfect axially compressed

cylinder with an axial crack", International Journal of Automotive and Mechanical Engineering, Vol. 14, No. 1, pp. 3837-3848, (2017).

[24] K. Yazdchi and A. R. Gowhari Anaraki, "Carrying capacity of edge-cracked columns under concentric vertical loads", Acta Mech, Vol. 198, pp. 1–19, (2008).

[25] Seyyed M. Hasheminejad, Behnam Gheshlaghi, Yaser Mirzaei and Saeed Abbasion, "Free transverse vibrations of cracked nanobeams with surface effects", Thin Solid Films, Vol. 519, No.8, pp. 2477-2482, (2011).

[26] W. Zhang, R. C. Picu, and N. Koratkar, "Suppression of fatigue crack growth in carbon nanotube composites", Appl. Phys. Lett. , Vol. 91, pp. 193109.1-193109.3, (2007).

[27] H. S. Rane, R.B. Barjibhe and A.V. Patil, "Free Vibration Analysis of Cracked Structure", International Journal on Mechanical Engineering and Robotics (IJMER), Vol. 2, No. 6, pp. 34-41, (2014).

[28] Jung-Chang Hsu, Haw-Long Lee and Win-Jin Chang, "Longitudinal vibration of cracked nanobeams using nonlocal elasticity theory", Curr. Appl Phys., Vol. 11, pp. 1384-1388 (2011).

[29] K.V. Singh, "Transcendental inverse eigenvalue problems in damage parameter estimation", Mech. Syst. Signal Process., Vol. 23, No. 6, pp. 1870-1883, (2009).

[30] Mustafa Özgür Yaylı and Ali Erdem Çerçevik, "Axial vibration analysis of cracked nanorods with arbitrary boundary conditions", J. Vibroeng., Vol. 17, No. 6, pp. 2907-2921, (2015).

[31] Masih Loghmani and Mohammad Reza Hairi Yazdi, "An analytical method for free vibration of multi cracked and stepped nonlocal nanobeams based on wave approach", Results Phys., Vol. 11, pp. 166-181, (2018).

[32] Farzad Ebrahimi and Fatemeh Mahmoodi , "Vibration analysis of carbon nanotubes with multiple cracks in thermal environment", Adv. Nano Res., Vol. 6, No. 1, pp 57-80, (2018).

[33] M. Dilena and A. Morassi, "The use of antiresonances for crack detection in beams", J. Sound Vib., Vol. 276, pp. 195–214, (2004).

[34] H. Tada, P.C.Paris and G.R.Irwin, The stress analysis of cracks handbook, ASME press, Newyork, (2000).

Appendix A: strain-displacement relation in tangential vibration

Considering scale effects, the relation between the microstrains and displacements up to three terms in the expansion can be written as:

$$\varepsilon_\alpha = \boldsymbol{\tau}_\alpha^0.\left(\boldsymbol{\tau}_\alpha^0.\nabla\boldsymbol{u}\right)+\frac{1}{2}\eta_\alpha\left[\boldsymbol{\tau}_\alpha^0.\left(\boldsymbol{\tau}_\alpha^0.\nabla\right)\left(\boldsymbol{\tau}_\alpha^0.\nabla\boldsymbol{u}\right)\right]+\frac{1}{6}\eta_\alpha^2\left[\boldsymbol{\tau}_\alpha^0.\left(\boldsymbol{\tau}_\alpha^0.\nabla\right)\left(\boldsymbol{\tau}_\alpha^0.\nabla\right)\left(\boldsymbol{\tau}_\alpha^0.\nabla\boldsymbol{u}\right)\right] \quad \text{(A1)}$$

The expressions for $\boldsymbol{\nabla}$,$\boldsymbol{\nabla u}$ and $\boldsymbol{\tau}_\alpha^0$ can be written in the cylindrical coordinates as:

$$\boldsymbol{\nabla}=\begin{bmatrix}\frac{\partial}{\partial r}\\ \frac{1}{r}\frac{\partial}{\partial\theta}\\ \frac{\partial}{\partial z}\end{bmatrix},\boldsymbol{u}=\begin{bmatrix}u_r\\ u_\theta\\ u_z\end{bmatrix},\boldsymbol{\nabla u}=\begin{bmatrix}\frac{\partial u_r}{\partial r} & \frac{1}{r}\left(\frac{\partial u_r}{\partial\theta}-u_\theta\right) & \frac{\partial u_r}{\partial z}\\ \frac{\partial u_\theta}{\partial r} & \frac{1}{r}\left(\frac{\partial u_\theta}{\partial\theta}+u_r\right) & \frac{\partial u_\theta}{\partial z}\\ \frac{\partial u_z}{\partial r} & \frac{1}{r}\frac{\partial u_z}{\partial\theta} & \frac{\partial u_z}{\partial z}\end{bmatrix},\boldsymbol{\tau}_\alpha^0=\begin{bmatrix}\tau_{\alpha r}^0\\ \tau_{\alpha\theta}^0\\ \tau_{\alpha z}^0\end{bmatrix} \quad \text{(A2)}$$

$$u_r=u_z=0,u_\theta=u_\theta(\theta) \quad \text{(A3)}$$

In the problem considered here, Eqs. (A3) are reduced to

$$\boldsymbol{\nabla}=\begin{bmatrix}0\\ 0\\ \frac{\partial}{\partial z}\end{bmatrix},\boldsymbol{u}=\begin{bmatrix}u_r\\ u_\theta\\ 0\end{bmatrix},\boldsymbol{\nabla u}=\begin{bmatrix}0 & -\frac{u_\theta}{r} & 0\\ 0 & \frac{1}{r}\frac{\partial u_\theta}{\partial\theta} & 0\\ 0 & 0 & 0\end{bmatrix},\boldsymbol{\tau}_\alpha^0=\begin{bmatrix}0\\ \tau_{\alpha\theta}^0\\ \tau_{\alpha z}^0\end{bmatrix} \quad \text{(A4)}$$

From Eq. (A4), $\boldsymbol{\tau}_\alpha^0.\boldsymbol{\nabla u}$ and $\boldsymbol{\tau}_\alpha^0.(\boldsymbol{\tau}_\alpha^0.\boldsymbol{\nabla u})$ can be written as:

$$\boldsymbol{\tau}_\alpha^0.\boldsymbol{\nabla u}=\frac{1}{r}\tau_{\alpha\theta}^0\begin{bmatrix}-u_\theta\\ \frac{\partial u_\theta}{\partial\theta}\\ 0\end{bmatrix} \quad \text{(A5)}$$

$$\boldsymbol{\tau}_\alpha^0.(\boldsymbol{\tau}_\alpha^0.\boldsymbol{\nabla u})=\frac{1}{r}(\tau_{\alpha\theta}^0)^2\frac{\partial u_\theta}{\partial\theta} \quad \text{(A6)}$$

Similarly, from Eq. (A4), it is concluded that

$$\boldsymbol{\nabla}(\boldsymbol{\tau}_\alpha^0.\boldsymbol{\nabla u})=\frac{1}{r^2}\tau_{\alpha\theta}^0\begin{bmatrix}0 & -2\frac{\partial u_\theta}{\partial\theta} & 0\\ 0 & \frac{\partial^2 u_\theta}{\partial\theta^2}-u_\theta & 0\\ 0 & 0 & 0\end{bmatrix} \quad \text{(A7)}$$

$$\boldsymbol{\tau}_\alpha^0.\boldsymbol{\nabla}(\boldsymbol{\tau}_\alpha^0.\boldsymbol{\nabla u})=\frac{1}{r^2}(\tau_{\alpha\theta}^0)^2\begin{bmatrix}-2\frac{\partial u_\theta}{\partial\theta}\\ \frac{\partial^2 u_\theta}{\partial\theta^2}-u_\theta\\ 0\end{bmatrix} \quad \text{(A8)}$$

$$\boldsymbol{\tau}_\alpha^0.(\boldsymbol{\tau}_\alpha^0.\boldsymbol{\nabla})(\boldsymbol{\tau}_\alpha^0.\boldsymbol{\nabla u})=\frac{1}{r^2}(\tau_{\alpha\theta}^0)^3\left(\frac{\partial^2 u_\theta}{\partial\theta^2}-u_\theta\right) \quad \text{(A9)}$$

$$\boldsymbol{\nabla}\left(\boldsymbol{\tau}_{\alpha}^{0}.\boldsymbol{\nabla}(\boldsymbol{\tau}_{\alpha}^{0}.\boldsymbol{\nabla}\boldsymbol{u})\right)=\frac{1}{r^{3}}(\tau_{\alpha\theta}^{0})^{2}\begin{bmatrix}0 & -3\frac{\partial^{2}u_{\theta}}{\partial\theta^{2}}+u_{\theta} & 0\\ 0 & \frac{\partial^{3}u_{\theta}}{\partial\theta^{3}}-3\frac{\partial u_{\theta}}{\partial\theta} & 0\\ 0 & 0 & 0\end{bmatrix} \tag{A10}$$

$$\boldsymbol{\tau}_{\alpha}^{0}.\left[\boldsymbol{\nabla}\left(\boldsymbol{\tau}_{\alpha}^{0}.\boldsymbol{\nabla}(\boldsymbol{\tau}_{\alpha}^{0}.\boldsymbol{\nabla}\boldsymbol{u})\right)\right]=\frac{1}{r^{3}}(\tau_{\alpha\theta}^{0})^{3}\begin{bmatrix}-3\frac{\partial^{2}u_{\theta}}{\partial\theta^{2}}+u_{\theta}\\ \frac{\partial^{3}u_{\theta}}{\partial\theta^{3}}-3\frac{\partial u_{\theta}}{\partial\theta}\\ 0\end{bmatrix} \tag{A11}$$

$$\boldsymbol{\tau}_{\alpha}^{0}.(\boldsymbol{\tau}_{\alpha}^{0}.\boldsymbol{\nabla})\left(\boldsymbol{\tau}_{\alpha}^{0}.\boldsymbol{\nabla}(\boldsymbol{\tau}_{\alpha}^{0}.\boldsymbol{\nabla}\boldsymbol{u})\right)=\frac{1}{r^{3}}(\tau_{\alpha\theta}^{0})^{4}(\frac{\partial^{3}u_{\theta}}{\partial\theta^{3}}-3\frac{\partial u_{\theta}}{\partial\theta}) \tag{A12}$$

Finally, if Eqs. (A6), (A9) and (A12) are substituted into Eq. (A1), it is found that

$$\epsilon_{\alpha}=\frac{1}{r}(\tau_{\alpha\theta}^{0})^{2}\frac{\partial u_{\theta}}{\partial\theta}+\frac{1}{2}\eta_{\alpha}\left[\frac{1}{r^{2}}(\tau_{\alpha\theta}^{0})^{3}(\frac{\partial^{2}u_{\theta}}{\partial\theta^{2}}-u_{\theta})\right]+\frac{1}{6}\eta_{\alpha}^{2}\left[\frac{1}{r^{3}}(\tau_{\alpha\theta}^{0})^{4}(\frac{\partial^{3}u_{\theta}}{\partial\theta^{3}}-3\frac{\partial u_{\theta}}{\partial\theta})\right] \tag{A13}$$

Substituting Eq. (A13) into Eq. (5) and the result in Eq. (6), yields

$$\sigma_{ij}^{(M)}=A_{0}\sum_{\alpha=1}^{3}\tau_{\alpha i}^{0}\tau_{\alpha j}^{0}\left\{\frac{1}{r}(\tau_{\alpha\theta}^{0})^{2}\frac{\partial u_{\theta}}{\partial\theta}+\frac{1}{12}\eta_{\alpha}^{2}\left[\frac{1}{r^{3}}(\tau_{\alpha\theta}^{0})^{4}(\frac{\partial^{3}u_{\theta}}{\partial\theta^{3}}-3\frac{\partial u_{\theta}}{\partial\theta})\right]\right\} \tag{A14}$$

If we set $i=j=\theta$ in Eq. (A14), we conclude that

$$\sigma_{\theta\theta}^{(M)}=A_{0}\sum_{\alpha=1}^{3}\left\{\frac{1}{r}(\tau_{\alpha\theta}^{0})^{4}\frac{\partial u_{\theta}}{\partial\theta}+\frac{1}{12}\eta_{\alpha}^{2}\left[\frac{1}{r^{3}}(\tau_{\alpha\theta}^{0})^{6}\left(\frac{\partial^{3}u_{\theta}}{\partial\theta^{3}}-3\frac{\partial u_{\theta}}{\partial\theta}\right)\right]\right\} \tag{A15}$$

If Eq. (A15) is substitute in Eq. (17) and Eqs. (25)- (30) is considered, we have

$$\frac{\partial N_{\theta\theta}^{(M)}}{\partial\theta}=\frac{Eh}{1-\nu^{2}}\sum_{\alpha=1}^{3}\left\{\frac{1}{r}\frac{\partial^{2}u_{\theta}}{\partial\theta^{2}}+\frac{1}{12}\eta_{\alpha}^{2}\left[\frac{1}{r^{3}}k\left(\frac{\partial^{4}u_{\theta}}{\partial\theta^{4}}-3\frac{\partial^{2}u_{\theta}}{\partial\theta^{2}}\right)\right]\right\} \tag{A16}$$

wherein $A_{0}=\frac{8}{9}\frac{E}{1-\nu^{2}}$ and For Zigzag $k=\frac{3}{4}$ and for Armchair $k=\frac{11}{12}$.